Full Paper

Propellants, Explosives, Pyrotechnics

DOI: 10.1002/prep.201400027

Ignition of Nanocomposite Thermites by Electric Spark and Shock Wave

William L. Shaw,[a] Dana D. Dlott,[a] Rayon A. Williams,[b] and Edward L. Dreizin*[b]

Abstract: Nanocomposite $8Al \cdot MoO_3$ thermite particles were prepared using arrested reactive milling and ignited using two experimental techniques. In spark ignition, a monolayer of powder was placed on a conductive substrate and heated in air by a pulsed electrostatic discharge. In shock ignition, an individual particle was targeted by a miniature, laser-driven flyer plate accelerated to a speed in the range of 0.5–2 $km\,s^{-1}$. In both experiments, time-dependent optical emission produced by the ignited material was monitored and recorded. The heating rates achieved in the present experiments are on the order of 10^{9-}–10^{11} $K\,s^{-1}$. These ignition methods result in a very fast combustion with characteristic burn times reduced by 1–3 orders of magnitude compared to the burn times measured previously for the same material ignited in the CO_2 laser beam, where it was heated at a much lower rate of about 10^{6-}–10^7 $K\,s^{-1}$. Ignition delays observed in both shock and spark ignition experiments are close to each other and vary in the range of 120–200 ns. The times of characteristic rapid increase in the optical emission of the ignited particles are also close to each other for the two experiments; however, these times are somewhat shorter (less than one μs) for the spark ignition tests compared to few μs observed for the shock initiated particles. Preliminary ideas enabling one to interpret the present results are discussed. This work establishes an approach for systematic studies of high rate ignition and respective combustion of nanocomposite reactive materials.

Keywords: Reactive materials · Energetic materials · Ignition delay · Burn time · Impact ignition · ESD ignition

1 Introduction

Composite materials containing components capable of highly exothermic reactions and mixed on the scale of 100 nm or finer have been developed for applications in explosives, propellants, and pyrotechnics [1]. A large surface area of the reactive interface associated with the nano-scale mixing between the fuel and oxidizer makes such materials sensitive to different ignition stimuli. Most of the quantitative measurements reported to date and characterizing reactions leading to ignition of reactive nanomaterials have relied on thermal analysis [2–10]. Measurements associated with faster processes have also been reported, including time-resolved mass spectrometry following ignition of nano-thermites [11–13], micro- [14] and nano-calorimetry [15,16], and measurements of optical emission and pressure generated by the material coated on an electrically heated filament [17,18]. In all of the above measurements, the heating rates were sufficiently low and the ignition delays were sufficiently long to ensure the temperature uniformity within the ignited nanocomposite structure. A model describing exothermic reactions for the thermally initiated, fully dense nano-thermite particles has been proposed quantifying individual reaction steps and predicting a thermal runaway to occur in vicinity of the experimental ignition temperature [19]. However, additional processes, including the release of oxygen prior to ignition [17,18,20–22] and a burst of ions produced by the rapidly heated nano-thermites [23], possibly associated with the oxygen release, have been reported but have not been well understood. Such processes can affect ignition and ensuing combustion of reactive nanomaterials; the effect may depend on the rate of heating and respective ignition delay.

Different ignition stimuli are expected to be important for different potential applications of the newly developed reactive nanomaterials. In particular, rapid initiation processes, such as electric spark or shock wave may produce a situation when the igniting nanomaterial is not uniformly heated; in addition, shocks may cause both bulk and local deformations, and fractures. Some parts of the sample may be substantially hotter than others, fresh direct contacts between fuel and oxidizer may be generated at the mechanically affected locations generating hot spots and leading to localized ignition. Such localized ignition may not necessarily be well described by the earlier kinetic models, dealing

[a] *W. L. Shaw, D. D. Dlott*
University of Illinois Urbana Champaign
Urbana, IL, USA

[b] *R. A. Williams, E. L. Dreizin*
New Jersey Institute of Technology
Newark, NJ, USA
**e-mail: dreizin@njit.edu*

with a homogeneously heated material. Furthermore, for the samples that are heated relatively slowly, the nanostructure may be lost when they burn and their temperature exceeds the melting points of the major components; conversely, the nanostructure may be preserved in very rapid reactions, occurring faster than the characteristic times required to change the material structure and morphology. Thus, the heating rate and the method of initiation of the nanocomposite reactive material may affect both its ignition kinetics and combustion dynamics.

In this paper, ignition of fully-dense, nanocomposite thermite particles prepared by Arrested Reactive Milling (ARM) [24] is studied experimentally using two methods leading to a very fast initiation. In one experiment, the particles placed on a conductive substrate are ignited using an electric spark (or an electro-static discharge, ESD). In the other experiment, the particles are struck by a supersonic flyer plate and are ignited as a result of the induced shock. In both cases, the observed ignition delays are of the order of 100 ns, which is insufficient for the temperature equilibration in the ignited particles. Results of both experiments are described and compared to each other. The implications of the present results are briefly discussed.

2 Material

The nanocomposite powder used in this work, metal-rich thermite $8Al \cdot MoO_3$ produced by ARM, has been used in several recent studies focused on its ignition and combustion [17, 25–27]. It was prepared using an aluminum powder, nominal particle size under 44 μm, 99.5 % purity by Atlantic Equipment Engineers and molybdenum oxide powder, nominal particle size under 44 μm, 99.95 % purity by Alfa Aesar. The starting powders were blended together and milled in hexane in an argon atmosphere for 30 min using a Retsch PM 400 MA planetary mill. Additional details characterizing the milling procedure and parameters are similar to those reported elsewhere [28].

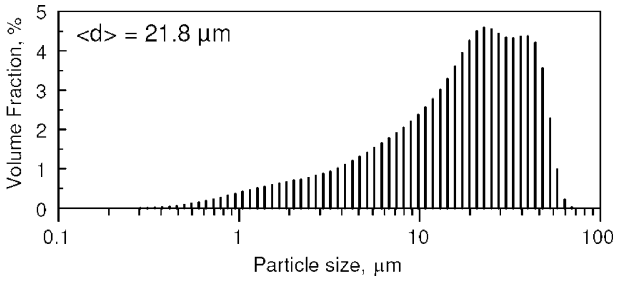

Figure 2. Particle size distribution for the prepared $8Al \cdot MoO_3$ nanocomposite powder.

A scanning electron microscope (SEM) image of the prepared powder particles is shown in Figure 1. The metal and oxidizer appear to be well mixed with no visible formation of aluminum oxide or reduced metallic phase. The material consists of irregularly shaped, roughly equiaxial composite particles ranging from about 0.5 to 50 μm. The particle size distribution obtained using a Beckman-Coulter LS230 Enhanced Particle Analyzer is shown in Figure 2, indicating 21.8 μm as the specific volumetric mean particle size.

3 Experimental Section

3.1 Spark Ignition

A detailed description of the experimental set up used for this work was given in Refs. [29, 30]. Figure 3 shows the apparatus including the Model 931 Firing Test System (FTS) by Electro-Tech Systems Inc., used to generate spark discharges.

A monolayer of $8Al \cdot MoO_3$ powder was used in all present experiments. A small amount of powder was placed on a double-sided carbon tape attached to an 18-mm diame-

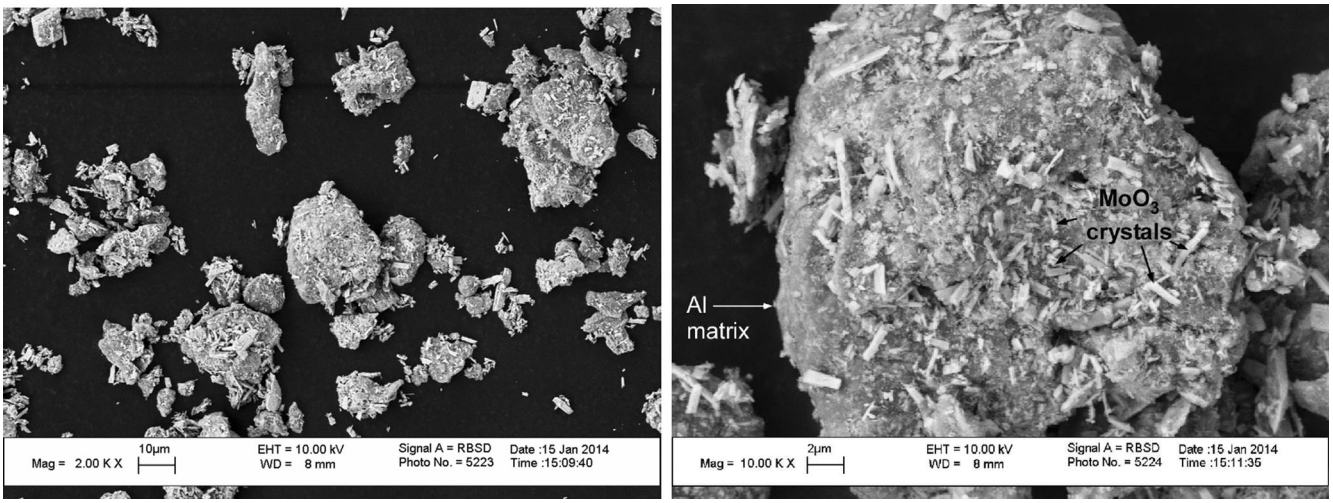

Figure 1. SEM images showing the particle shapes and surface morphology for the prepared $8Al \cdot MoO_3$ nanocomposite powder.

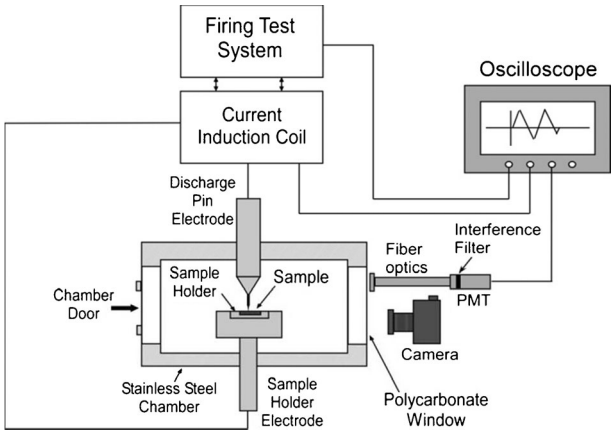

Figure 3. Schematic of the experimental set-up for ESD ignition.

ter custom-made polished brass support. Excess powder was blown away, and the powder remaining on the tape formed a monolayer, as was confirmed by inspection of the prepared samples using an SEM. The sample holder was grounded. A needle-electrode was fixed approximately 0.2 mm above the powder surface, following a standard methodology (MIL-STD-1751A). A spark was triggered using FTS. All experiments were performed in room air.

The discharges with different energies were produced using a 2000-pF capacitor charged to a voltage varied from 3 to 8 kV. Typically, five experiments were performed for each voltage.

An inductance coil model 110 A with a 1 V/10 A ratio by Pearson Electronics was used to measure the spark current. Current traces were recorded by a LeCroy WaveSurfer 64Xs Series oscilloscope. As in the previous work [29], the powder resistance, R_p, was determined based on the current traces recorded for the same ESD settings for the sample holders with and without powder. For each experiment, the current trace, showing a decaying oscillatory pattern, was matched with that calculated for an *R-C* circuit connected in series (where the capacitance, $C = 2000$ pF). The traces were matched to each other by adjusting the circuit impedance, *R*, so that the equivalent resistance for each experiment was obtained. The circuit impedance was assumed to remain constant during the discharge. The current traces were matched with a 95% confidence interval. The difference between resistances for the powder-loaded and empty sample holders was assumed to represent R_p. Joule heating energy was obtained by numerical integration of $I^2(t)R_p\Delta t$, where *I* is the recorded ESD current, *t* is time, and Δt is the time step of the data acquisition.

In all present experiments, ignition was accompanied by multiple streaks of ejected and individually burning particles. The emission produced by the igniting powder was measured with a Hamamatsu, H3164-10 photomultiplier tube (PMT) with 0.8 ns rise time equipped with a 486-nm interference filter. The PMT output was recorded with a LeCroy WaveSurfer 64Xs Series oscilloscope.

3.2 Shock Experiment

3.2.1 Apparatus

Aluminum laser-driven flyer plates were used to shock individual 10–20 μm $8Al \cdot MoO_3$ thermite particles, and the resulting optical emission was time resolved. The apparatus for launching laser-driven flyer-plates, shown schematically in Figure 4a, has been described previously [31]. Using homogeneous flat top laser pulses with up to 2500 mJ energies, we launched 50 μm thick, 700 μm diameter aluminum flyer plates from a sheet of Al 1145 foil epoxied to a glass window [31]. The Al disks fly in vacuo across a 350 μm gap before colliding with the target. As they fly, the edges of the plates become distorted, but upon impact the flyers have an estimated 160 μm diameter planar region in the center, much larger than the target particles. This type of impact process produces a planar shock in the thermite particles. The shock duration is dependent on the material being impacted, but with the flyers used here, the duration was about 10 ns.

The targets consisted of $8Al \cdot MoO_3$ thermite particles adhered to a glass window by a thin layer of cement. The targets were prepared by spin coating a 0.75 μm thick layer of UV curable acrylic cement (Dymax 401) onto a 6.35-mm thick BK7 glass window. The $8Al \cdot MoO_3$ thermite powder, suspended in hexane, was deposited onto a glass slide and the hexane was allowed to evaporate. The thermite was then tapped off the slide onto the cement layer. A UV lamp was used to cure the glue and fix the particles, while the sample was attached to a spin coater. The quantity of thermite was chosen so that the thermite layer was mainly in

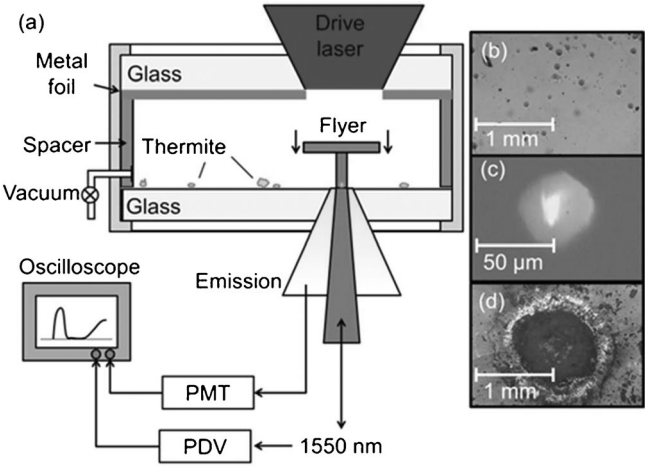

Figure 4. (a) Schematic of the laser-driven flyer plate system. (b) Image of a thermite target, consisting of many individual particles scattered on an optical window. A thin 0.75 μm layer of cement was used to fix the particles. (c) Microscope image of a 20 μm $8Al \cdot MoO_3$ thermite particle through a 50 μm aperture. (d) Reacted thermite in the center of a crater created by impact with a 700 μm diameter Al flyer plate.

the form of isolated individual particles. A microscope image of a typical target is shown in Figure 4b.

This apparatus (Figure 4a) allows us to target an individual, size-selected thermite particle, launch a flyer plate at a selected velocity, monitor the velocity history of the flyer, and detect the time-resolved emission from the shocked thermite. The velocity histories of the flyer plates were measured using a photonic Doppler velocimeter (PDV) [32, 33] operating at 1550 nm laser wavelength [31]. The PDV was detected by electronics, including a digital oscilloscope, with a combined bandwidth of 7.4 GHz, which is capable of monitoring speeds up to 5.4 $km\,s^{-1}$. The PDV data were analyzed using a short-time Fourier transform analysis. There was an estimated 1 ns uncertainty in measuring the timing of flyer impact.

A 10× microscope objective and a dichroic beamsplitter was used to observe the thermite particles, direct the PDV beam onto the flyer, collect the returned PDV signals, and collect the thermite emission. The PDV beams were collimated and 60 μm in diameter, so enough of the PDV beam passed by the thermite particles (Figure 4a) to monitor the flyer plates.

In our apparatus, we could insert a mirror (not shown) that allowed us to observe the target with a homebuilt video microscope. We translated the target until a particle of suitable size was centered in the image, and we stopped down an iris to so that we observed only the 50 μm diameter region immediately adjacent to the selected single thermite particle. An image of a roughly 20 μm thermite particle within the iris aperture is shown in Figure 4c. We then removed the mirror and directed light from the thermite particle into a photomultiplier tube (Hamamatsu, H10720-20) with a 0.8 ns rise time. The PMT signals were digitized using the same oscilloscope that detected the PDV signals. The photomultiplier tube (PMT) and PDV time delays were determined using a method detailed previously [31]. This synchronization procedure involved simultaneous measurements of 10 ns laser pulses by both devices, and we have estimated the synchronization error between flyer impact and emission risetime to be 5 ns.

We should note that when we cite the size of the irregularly-shaped thermite particles, we refer to the diameter of the minimum circle that could be circumscribed around the particle image. Thus particles with the same cited diameter may have significantly different masses and volumes.

3.2.2 Shock-Particle Interaction

When the laser-driven flyer-plate impacts a particle, the pressure, density, and temperature of the particle jump as the shock front passes through the sample. We do not have an accurate equation-of-state for these thermite particles, or a truly accurate way to describe a shock in such a nanostructured medium. However, we can illustrate the shock properties by describing what would happen if the particles were pure Al and unreactive, and the flyer speeds were either 1 $km\,s^{-1}$ or 2 $km\,s^{-1}$. Using the well-known Hugoniot-crossing method [34] and the principal Hugoniot of Al [35], we find that with a 1 $km\,s^{-1}$ flyer, the shock transit time across a 20 μm thick particle would be 3.5 ns, the pressure would be 8.2 GPa and the compression would be 8.5%. Following a calculation previously presented [36], we can also estimate the peak temperature during the shock. With a 1 $km\,s^{-1}$ flyer, a particle initially at 300 K would be briefly heated to 366 K. The corresponding values for a 2 $km\,s^{-1}$ flyer would be 3.1 ns transit time, 17.8 GPa pressure, 15% compression, and 493 K. These conditions are crude estimates for the temperatures of shocked thermite particles on short times scales that precede the onset of exothermic reactivity. Given that it takes only 3.1 ns for the particle to be shocked, the heating rate is close to $6.3\times10^{10}\,K\,s^{-1}$.

In the actual shocked thermite particles there may be multiple shock reverberations at the interfaces between grain boundaries. There may be defects or voids, which the shock may collapse. There may be frictional heating at moving edge dislocations. There will be reflections from the thermite-glue-glass interface. All these factors can create nanometric regions with transient temperatures that exceed the bulk temperature rises, i.e. the complicated nanostructure and microstructure of the thermite particles can promote the creation of hot spots.

Figure 4d shows an image of a target after the 20 μm particle shown in Figure 4c was impacted by the 700 μm diameter flyer plate at 1 $km\,s^{-1}$. Besides the Al crater left over from the flyer plate, one can see a smaller faint image in the central region that is about the same size as the original thermite particle. We believe this region denotes debris from the shock-reacted thermite particle.

4 Results

4.1 ESD Ignition of 8Al·MoO3 Monolayers

Ignition experiments carried out for $8Al\cdot MoO_3$ powder monolayers always produced multiple burning particles resulting in an emission signal similar to that shown in Figure 5. An initial fast rise is followed by slower increasing emission intensity. The slow rise segment becomes more apparent and extends to longer times at greater spark energies. The time axis is broken between 30 and 90 μs, while the signal continues to decrease. The overall duration of the recorded emission signal, corresponding to the time of combustion varied from ca. 120 to 200 μs and did not apparently depend on the spark energy. These times are determined from the emission traces, such as shown in Figure 5, while the signals exceeded three times the amplitude of fluctuations observed at the zero emission level (prior to the spark). Images in Figure 6 show a photograph of burning particle streaks observed in a typical experiment and partially burned particles captured on a Cu foil placed approximately 2 mm from the powder.

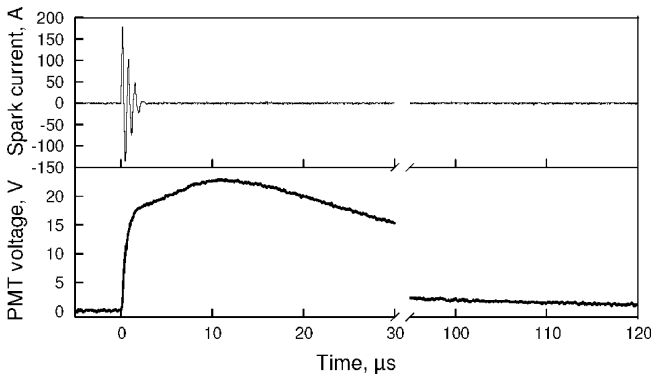

Figure 5. An ESD spark current trace and a PMT voltage corresponding to the emission of the burning sample recorded in an ignition test with a monolayer of nanocomposite $8Al \cdot MoO_3$ powder. The spark voltage is 8 kV.

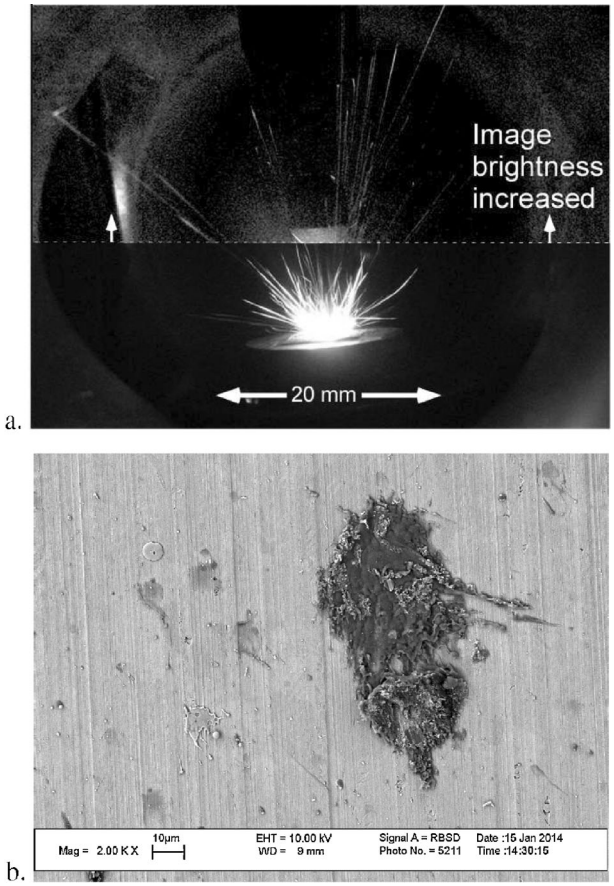

Figure 6. (a) A photograph of the burning particle streakes recorded in an ESD ignition test with the spark voltage of 8 kV. (b) An SEM image taken with backscattered electrons showing partially burned particles captured on a Cu foil placed 2 mm away from the spark-ignited powder.

In the photograph, the brightness and contrast for the top part are additionally enhanced to clarify the images of few particle streaks extending beyond the brightest area of the image. The maximum streak length is close to 50 mm. Considering the overall emission time of about 150–200 μs, this suggests that the fastest burning particles move at a speed of about 300 $m\,s^{-1}$, approaching the speed of sound in air. This could indicate that the particles are carried by the spark-generated shock.

The partially burned particles captured on the Cu foil appear molten and form splattered imprints on the surface. The sizes of the captured particles change in a wide range, which appears to be similar to the original size distribution of the nanocomposite thermite (see Figure 2). A large particle with portions containing what appears to be a composite structure similar to the original nanocomposite material is seen on the right. Multiple smaller particles are seen on the left, for which almost no internal structure could be resolved.

A close inspection of the recorded spark current and emission traces showed that the onset of the emission signal is delayed compared to the spark current. These delays are clearly observed in Figure 7, showing the initial parts of the emission traces overlapped with the respective ESD current signals. These short delays were ignored in an earlier paper [37] where the focus was on much longer ignition delays observed when the powder was placed in a thick layer and ignited after an aerosolized cloud of the ejected particles was formed.

The emission signals were further processed to obtain ignition delays defined as the difference between onset times for the spark current and PMT voltage, 90% of the fast rise time for the PMT signal, and integrated emission intensities determined using the PMT voltage traces. For consistency the onset instants for the current signals were defined when their values were at 10% of the maximum. The 10% and 90% values of the fast rise represents 10% and 90% of the time difference between the onset of the emission signal and the inflection point between its fast

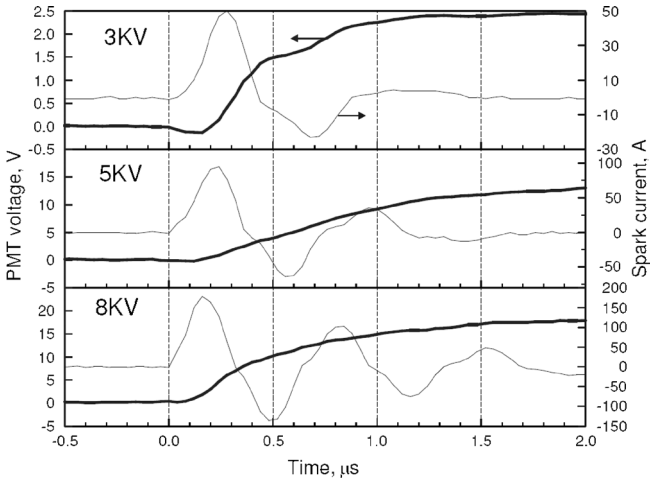

Figure 7. Optical emission and spark current traces showing onset differences for $8Al \cdot MoO_3$ powder monolayer ignited at different ESD energies.

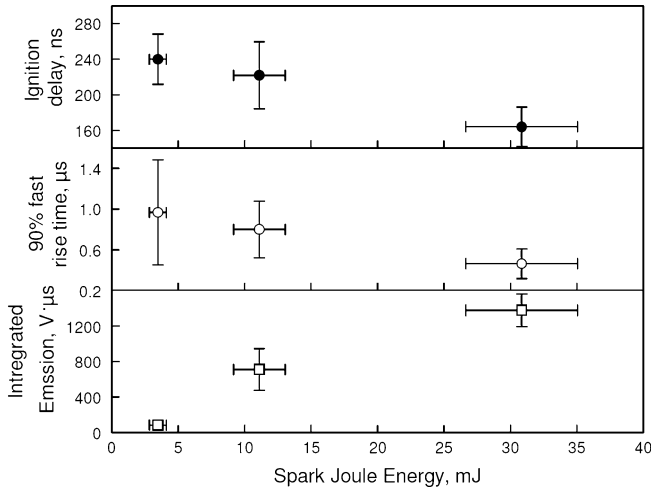

Figure 8. Ignition delay, 90% fast rise time and integrated emission as a function of Joule energy for $8Al \cdot MoO_3$ powder monolayer ignited by spark.

and slow rise segments, respectively. The results of the processing are shown in Figure 8 as a function of the spark's Joule energy. The Joule energy was consistently increased at greater spark voltages.

The ignition delay decreases from ca. 240 to 160 ns with the increase in the spark's energy. Similarly, a reduction in the 90% fast rise time was observed with the increasing energy. Integrated emission intensities showed an opposite trend and were observed to increase at greater spark energies.

4.2 Shock Ignition of Individual $8Al \cdot MoO_3$ Particles

A time-resolved emission transient for the impact velocity of 1.34 km s^{-1} is plotted in Figure 9. Time zero is the moment of flyer impact measured by PDV with a 5 ns uncertainty. In addition, the flyer plate speed as measured by PDV is shown. Below flyer speeds of ca. 0.5 km s^{-1}, there were no obvious signs of thermite emission, but above 0.5 km s^{-1} the thermite particles produced intense emission

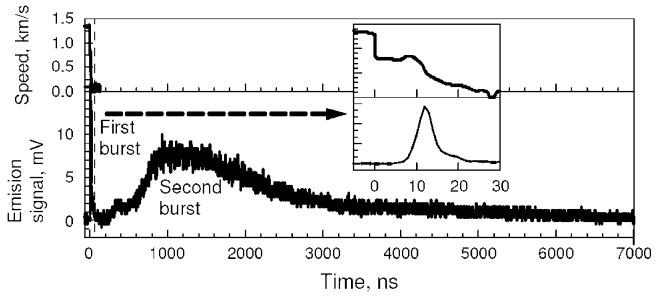

Figure 9. Characteristic shock induced emission trace and flyer speed as a function of time for a 10–20 µm $8Al \cdot MoO_3$ particle. The impact velocity is 1.34 km s^{-1}.

bursts, so 0.5 km s^{-1} is taken as an impact velocity ignition threshold. This velocity threshold almost certainly depends on the shock duration as controlled by flyer thickness, and might be lower for thicker flyers.

Above this velocity threshold, the emission transients consist of two bursts, with the first burst lasting 30 ns, followed by a delay of a few hundred ns and a second burst lasting a few µs. As the flyer plate impact velocity was increased, the intensity of both bursts increased. The first, short high amplitude burst and flyer speed are shown with and expanded time scale in the inset in Figure 9. The PDV data show the flyer at $t<0$ moving at constant speed through the vacuum. Abruptly at $t=0$ the flyer speed declines due to the impact. After this initial decline there is a 10 ns period of constant velocity when the shock is steady. Following this 10 ns shock, the flyer undergoes a more gradual deceleration over ca. 30 ns. Figure 9 shows that the rapid rise of the first emission burst is coincident with the flyer impact. The initial emission burst ends at about the time the flyer comes to rest or perhaps slightly later and has been discussed in a previous publication [38]. Note that because the flyer is made of a solid slab of oxide-passivated Al and contains no oxidizer, participation of the flyer metal in the redox reaction is highly unlikely. Thus the entire measured emission signal exceeding the background level observed with inert targets is attributed to the reaction of the thermite particle.

Figure 10 shows the emission intensities for three different impact velocities. As the flyer speeds increase, the onset of the second burst moves to shorter time and the rise of the second burst becomes faster. We did a number of experiments where flyers impacted only glass, or only glass and acrylic cement. Although there was a detectable amount of emission from these other materials, the emission intensities from impacted thermite particles vastly exceeded that of glass or acrylic cement. The signal from the cement and glass was undetectable during the time the first short burst was observed for the thermite particle. The signal rose and showed a detectable baseline during the

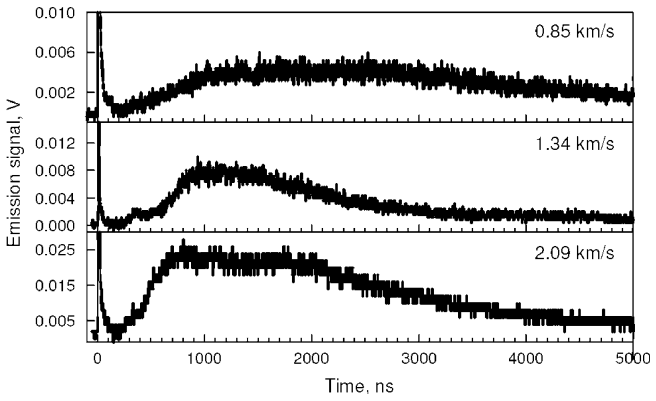

Figure 10. Emission traces for $8Al \cdot MoO_3$ particles ignited by impacts at different speeds.

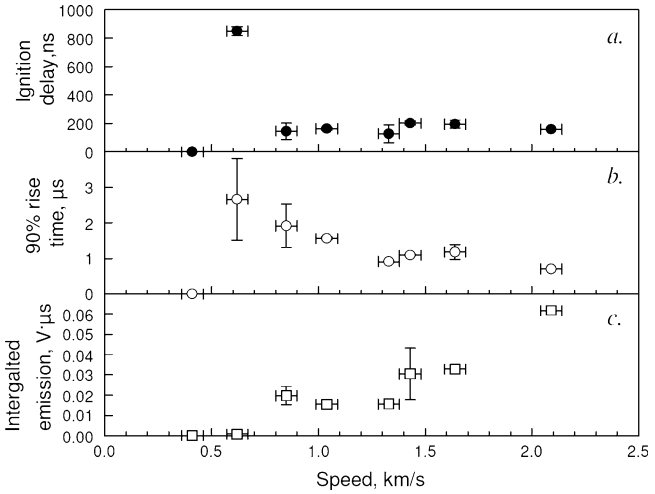

Figure 11. Properties of the second emission burst as a function of flyer impact speed. (a) Delay is the time between impact at t = 0 and the 10% point of the second burst rise. (b) Rise time is the time for 10–90% rise of the emission burst. (c) Integral is proportional to the time-integrated emission burst intensity.

time the second burst was observed. The amplitude of the baseline was about 15 times smaller than the signal produced by an ignited thermite particle.

In Figure 11 we show the flyer-speed dependence of three properties of the second emission bursts, the time delays between impact and the second bursts (Figure 11 a), the risetimes (10–90%) of the second bursts (Figure 11 b), and the integrated areas of the second bursts (Figure 11 c). The time delay is the time when the second emission burst reaches 10% of its maximum. The risetime is the 10–90% rise of the second emission burst.

The ignition delay stay in a narrow range of ca. 150–200 ns for all except the lowest impact energy, for which the delay is much longer. The risetime is consistently decreasing and the integrated signal increasing with the impact energy.

5 Discussion

5.1 Heating Times and Burn Rates

Both initiation techniques considered herein result in very fast heating of the nanocomposite thermite particles. A simple estimate discussed above for the shock initiation indicates the heating rate on the order of 10^{10-}–10^{11} K s^{-1}. Although the temperature achieved as a result of shock compression is relatively low, as mentioned above, localized hot spots with substantially greater temperature are likely to be formed; for those even greater heating rates are expected. For the spark ignition experiment, the heating rate can be roughly estimated assuming that the emission signal becomes noticeable at 486 nm when at least portions of the material are heated to ca. 1000 K. Because this occurs after the delays varied around 150–250 ns (see Figure 8), the heating rates are estimated to be $0.5–1 \times 10^{10}$ K s^{-1}. For spark ignition, the heating occurs locally because most of the heat release occurs at the points of maximum resistance, i.e., at the contact between the conductive substrate and the particle. For the composite material, it is also possible that the Joule energy is partially released at heterogeneities and material boundaries within the particle. The time required for the temperature to equilibrate within a 10-μm aluminum particle is estimated to be approximately 1 μs, which is much longer than any of the ignition delays reported herein. An even longer thermal equilibration time is anticipated for the composite particle. Thus, if local hot spots are formed in the impact or spark initiated particles, it is likely that the ignition is also localized and combustion begins around those hot spots.

A very rapid initiation with the characteristic ignition (and thus local heating) times shorter than the time required for the temperature equilibration within the particle appears to be the principle difference between the present experiments and laser ignition measurements reported for the same material recently [27]. When the particle was heated while passing through a CO_2 laser beam, its heating time was close to 50–70 μs and the heating rates were on the order 10^{6-}–10^{7} K s^{-1}. Thus, the particle temperature was uniform before its ignition and, likely, during its combustion. Remarkably, the burn times reported in Ref. [27] are of the order of several ms, much longer than the present data: few μs for the shock ignition and 120–200 μs for the spark ignition. Note that in spark ignition experiments multiple particles are ignited and the measured emission time characterizes combustion of the largest particles ignited after the longest delays. In other words, the actual particle combustion times in the spark ignition experiments were likely noticeably shorter than the entire duration of the measured emission signal.

The difference in burn times observed here and in laser ignition experiments is likely associated with the mode of combustion. When laser ignited particles are heated above the melting point of aluminum, it is likely that the nanostructure present in the starting material disappears and the particle burns as a molten drop of aluminum attached to a solid or molten particle of MoO_3. A relevant rapid loss of nanostructure upon heating of agglomerated nanoparticles of aluminum was documented in Ref. [39]. It was reported to begin above 1300 K for oxide-passivated Al nanoparticles. The characteristic nanostructure loss times and temperatures may be different for the fully-dense nanocomposite particles addressed here. It is suggested that the characteristic ignition times in the present experiments are so short that the nanostructure of the starting material may be preserved. In this case, the reaction will be driven by heterogeneous diffusion of components occurring over a very large surface area existing in the nanocomposite material. The rapid rise in temperature causes this reaction to accelerate dramatically before a finite product layer be-

tween Al and MoO_3 is grown, which could lead to the very short reaction times observed. Note also that in the shock ignition experiment, the flyer plate remains in contact with the particle, which could quench the reaction before its completion. Additional work is necessary to fully understand the present combustion mechanisms.

5.2 Ignition Delays and Emission Rise Times

In shock ignition, the observed ignition delay corresponds roughly to the timing of transverse decompression waves from the flyer plate [36]. These generate shear forces, which might initiate a reaction in $8Al \cdot MoO_3$ nanocomposite material. It is intriguing that the ignition delays observed in both shock and spark ignition experiments (see Figure 8 and Figure 11) are close to each other. Thus, these delays may represent an intrinsic time necessary for the heterogeneous reaction to accelerate in this material. This time must be a function of the chemical composition and structure. Experiments with different materials would be useful in clarifying the processes governing the observed ignition delays in both experiments.

Similarly, it is interesting to compare the rise times for the optical signals observed in both experiments. Because the spark cathode and anode spots are reported to be in the range of several μm [40, 41], it is likely that the spark directly heats one particle initially; after that particle ignites, the heating propagates to the rest of the sample. The rapid emission ramp is likely to be indicative of the ignition of the particle directly heated by the spark; the slower rising part of the emission signal characterizes the reaction propagation to the rest of the sample (see Figure 5). The rise times presented in Figure 8 and Figure 11 are close to each other; however, they are somewhat shorter for the spark ignition tests. If these times represent ignition of an individual particle, the shorter times for the spark ignition tests can be readily interpreted recalling that the electrostatic discharge remains active during this time, while the shock loading of the particle has been completed. In addition, as noted above, the shock ignited particles remain in contact with the flyer plate, resulting in additional heat losses, although such losses are relatively small for the short times considered.

5.3 Ignition Temperatures

An ignition delay reported in Figure 8 can be used to estimate the initial particle temperature for the spark ignition tests. This estimate must assume the homogeneous particle heating; thus the temperatures achieved in the hot spots are expected to be higher. The temperature was estimated considering an adiabatic Joule heating of a particle with diameter equal to the mean volumetric particle size of 21.8 μm during the 150–240 ns ignition delay. The real-time recorded spark current signal was used, and the powder impedance was assumed to remain constant. The results of this estimate are shown in Figure 12. Estimated temperatures compare well with the range of 800–900 K, for which ignition of the same $8Al \cdot MoO_3$ powder is observed when it is coated on an electrically heated wire [17, 18]. Based on this estimate, it is reasonable to expect that such heterogeneous reactions as considered in the multi-step ignition model for a similar nanocomposite thermite [19] are also active in the present experiments. However, because of the lack of pre-ignition reactions, Al and MoO_3 remain in nearly intimate contact, and the rate of these reactions can be substantially increased.

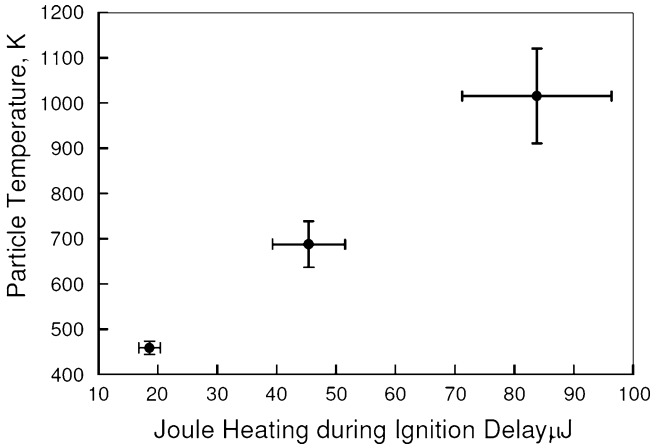

Figure 12. Estimated temperature to which the volumetric mean particle size is heated by the spark current during the delay time for $8Al \cdot MoO_3$ powder monolayer.

6 Conclusions

Nanocomposite $8Al \cdot MoO_3$ thermite particles with μm-sized dimensions were ignited using both shock compression and spark ignition techniques with very high heating rates on the order of 10^{9-}–10^{11} $K s^{-1}$. These ignition methods result in a very fast combustion with characteristic burn times reduced by 1–3 orders of magnitude compared to the burn times measured previously for the same material ignited in the CO_2 laser beam [27], where it was heated at a much lower rate of about 10^{6-}–10^{7} $K s^{-1}$. It is proposed that the greater burn rates achieved after a very rapid ignition are associated with the preserved nanostructure and respectively very high heterogeneous reaction rate achieved at the high combustion temperatures. Ignition delays observed in both shock and spark ignition experiments are close to each other and vary in the range of 120–200 ns. The times of characteristic rapid increase in the optical emission of the ignited particles are also close to each other for the two experiments; however, these times are somewhat shorter (less than one μs) for the spark ignition tests compared to few μs observed for the shock initiated particles. The spark-ignited nanocomposite thermite particles are observed to be ejected from the substrate at the

speeds approaching the speed of sound in surrounding air. The mechanisms of processes responsible for the measured ignition delays, emission rise times, combustion duration, and particle ejection by the spark will be investigated in future experiments, in which the range of materials tested will be expanded.

Acknowledgments

The research described here was based on work supported by the US Army Research Office under awards W911NG-13-0217 (DDD) and W911NF-12-1-0161 (ELD), and the US Defense Threat Reduction Agency (DTRA) under award HDTRA1-12-1-0011 (DDD). William L. Shaw acknowledges support from the Stewardship Science Academic Alliance Program (Carnegie-DOE Alliance Center) under award DE-NA002006.

References

[1] E. L. Dreizin, Metal-Based Reactive Nanomaterials, *Prog. Energy Combust. Sci.* **2009**, *35*, 141.
[2] D. Stamatis, E. L. Dreizin, Thermal Initiation of Consolidated Nanocomposite Thermites, *Combust. Flame* **2011**, *158*, 1631.
[3] A. Ermoline, M. Schoenitz, E. L. Dreizin, Reactions Leading to Ignition in Fully Dense Nanocomposite Al-Oxide Systems, *Combust. Flame* **2011**, *158*, 1076.
[4] C. Farley, M. Pantoya, Reaction Kinetics of Nanometric Aluminum and Iodine Pentoxide, *J. Therm. Anal. Calorim.* **2010**, *102*, 609.
[5] B. R. Clark, M. L. Pantoya, The Aluminium and Iodine Pentoxide Reaction for the Destruction of Spore Forming Bacteria, *Phys. Chem. Chem. Phys.* **2010**, *12*, 12653.
[6] Y. Wang, C. Yang, X. L. Song, W. Jiang, G. D. Deng, F. S. Li, Reactive Materials Synthesis and Aluminothermy Reaction of Aluminum/cobalt Lead Oxide, *Appl. Mech. Mater.* **2013**, *320*, 383.
[7] Y. Yang, D. Xu, K. Zhang, Effect of Nanostructures on the Exothermic Reaction and Ignition of Al/CuO_x-Based Energetic Materials, *J. Mater. Sci.* **2012**, *47*, 1296.
[8] Y. Wang, X. Song, W. Jiang, G. Deng, X. Guo, H. Liu, F. Li, Synthesis of Nano-Nickel-Coated Micro-Aluminum and Thermal Reactivity of Aluminum/Nickelstannic Oxide Thermite, *Int. J. Energ. Mater. Chem. Propul.* **2011**, *10*, 231.
[9] J. Wang, A. Hu, J. Persic, J. Z. Wen, Y. Norman Zhou, Thermal Stability and Reaction Properties of Passivated Al/CuO Nanothermite, *J. Phys. Chem. Solids* **2011**, *72*, 620.
[10] M. Petrantoni, C. Rossi, L. Salvagnac, V. Conédéra, A. Estève, C. Tenailleau, P. Alphonse, Y. J. Chabal, Multilayered Al/CuO Thermite Formation by Reactive Magnetron Sputtering: Nano vs. Micro, *J. Appl. Phys.* **2010**, *108*, 084323.
[11] K. T. Sullivan, C. Wu, N. W. Piekiel, K. Gaskell, M. R. Zachariah, Synthesis and Reactivity of Nano-Ag_2O as an Oxidizer for Energetic Systems Yielding Antimicrobial Products, *Combust. Flame* **2013**, *160*, 438.
[12] L. Zhou, N. Piekiel, S. Chowdhury, M. R. Zachariah, Time-resolved Mass Spectrometry of the Exothermic Reaction between Nanoaluminum and Metal Oxides: The Role of Oxygen Release, *J. Phys. Chem. C* **2010**, *114*, 14269.
[13] G. Jian, N. W. Piekiel, M. R. Zachariah, Time-Resolved Mass Spectrometry of Nano-Al and Nano-Al/CuO Thermite under Rapid Heating: A Mechanistic Study, *J. Phys. Chem. C* **2012**, *116*, 26881.
[14] N. W. Piekiel, R. E. Cavicchi, M. R. Zachariah, Rapid Heating of Energetic Materials Using a Micro-Differential Scanning Calorimeter, *Thermochim. Acta* **2011**, *521*, 125.
[15] P. Swaminathan, M. D. Grapes, K. Woll, S. C. Barron, D. A. Lavan, T. P. Weihs, Studying Exothermic Reactions in the Ni-Al System at Rapid Heating Rates Using a Nanocalorimeter, *J. Appl. Phys.* **2013**, *113*, 143509.
[16] M. Vohra, M. Grapes, P. Swaminathan, T. P. Weihs, O. M. Knio, Modeling and Quantitative Nanocalorimetric Analysis to Assess Interdiffusion in a NiAl Bilayer, *J. Appl. Phys.* **2011**, *110*, 123521.
[17] R. A. Williams, J. V. Patel, A. Ermoline, M. Schoenitz, E. L. Dreizin, Correlation of Optical Emission and Pressure Generated upon Ignition of Fully-dense Nanocomposite Thermite Powders, *Combust. Flame* **2013**, *160*, 734.
[18] R. A. Williams, M. Schoenitz, A. Ermoline, E. L. Dreizin, On Gas Release by Thermally-Initiated Fully-Dense 2Al•3CuO Nanocomposite Powder, *Int. J. Energ. Mater. Chem. Propul.* **2012**, *11*, 275.
[19] D. Stamatis, A. Ermoline, E. L. Dreizin, A Multi-Step Reaction Model for Ignition of Fully-Dense Al•CuO Nanocomposite Powders, *Combust. Theor. Model.* **2012**, *16*, 976.
[20] K. T. Sullivan, N. W. Piekiel, S. Chowdhury, C. Wu, M. R. Zachariah, C. E. Johnson, Ignition and Combustion Characteristics of Nanoscale Al/AgIO 3: A Potential Energetic Biocidal System, *Combust. Sci. Technol.* **2011**, *183*, 285.
[21] K. Sullivan, M. R. Zachariah, Simultaneous Pressure and Optical Measurements of Nanoaluminum Thermites: Investigating the Reaction Mechanism, *J. Propul. Power* **2010**, *26*, 467.
[22] G. Jian, S. Chowdhury, K. Sullivan, M. R. Zachariah, Nanothermite Reactions: Is Gas Phase Oxygen Generation from the Oxygen Carrier an Essential Prerequisite to Ignition?, *Combust. Flame* **2013**, *160*, 432.
[23] L. Zhou, N. Piekiel, S. Chowdhury, D. Lee, M. R. Zachariah, Transient Ion Ejection during Nanocomposite Thermite Reactions, *J. Appl. Phys.* **2009**, *106*, 083306.
[24] E. L. Dreizin, M. Schoenitz, Nano-Composite Energetic Powders Prepared by Srrested Reactive Milling, US Patent 7,524,355, **2009**.
[25] S. M. Umbrajkar, S. Seshadri, M. Schoenitz, V. K. Hoffmann, E. L. Dreizin, Aluminum-Rich Al-MoO_3 Nanocomposite Powders Prepared by Arrested Reactive Milling, *J. Propul. Power* **2008**, *24*, 192.
[26] D. Stamatis, E. L. Dreizin, K. Higa, Thermal Initiation of Al-MoO_3 Nanocomposite Materials Prepared by Different Methods, *J. Propul. Power* **2011**, *27*, 1079.
[27] E. L. Dreizin, C. Badiola, S. Zhang, Y. Aly, Particle Combustion Dyanmics of Metal-Based Reactive Materials, *Int. J. Energ. Mater. Chem. Propul.* **2011**, *10*, 22.
[28] D. Stamatis, Z. Jiang, V. K. Hoffmann, M. Schoenitz, E. L. Dreizin, Fully Dense, Aluminum-Rich Al-CuO Nanocomposite Powders for Energetic Formulations, *Combust. Sci. Technol.* **2009**, 181, 97.
[29] E. Beloni, E. L. Dreizin, Experimental Study of Ignition of Magnesium Powder by Electrostatic Discharge, *Combust. Flame* **2009**, *156*, 1386.
[30] E. Beloni, E. L. Dreizin, Ignition of Aluminum Powders by Electrostatic Discharge, *Combust. Flame* **2010**, *157*, 1346.
[31] K. E. Brown, W. L. Shaw, X. X. Zheng, D. D. Dlott, Simplified Laser-Driven Flyer Plates for Shock Compression Science, *Rev. Sci. Instrum.* **2012**, *83*, 103901.
[32] M. D. Bowden, M. P. Maisey, The Development of a Heterodyne Velocimeter System for Use in Sub-Microsecond Time Regimes, *Proc. SPIE* **2007**, *6662*, 66620B.

[33] J. D. Weng, X. Wang, Y. Ma, H. Tan, L. C. Cai, J. F. Li, C. L. Liu, A Compact all-Fiber Displacement Interferometer for Measuring the Foil Velocity Driven by Laser, *Rev. Sci. Instrum.* **2008**, *79*, 113101.

[34] J. W. Forbes, *Shock Wave Compression of Condensed Matter: A Primer*, Springer, New York, **2012**, p. 147.

[35] S. P. Marsh, *LASL Shock Hugoniot Data*, University of California Press, Berkeley, **1980**, p. 165.

[36] X. X. Zheng, A. D. Curtis, W. L. Shaw, D. D. Dlott, Shock Initiation of Nano-Al plus Teflon: Time-Resolved Emission Studies, *J. Phys. Chem. C* **2013**, *117*, 4866.

[37] R. A. Williams, J. V. Patel, E. L. Dreizin, Ignition of Fully Dense Nanocomposite Thermite Powders by an Electric Spark, *J. Propul. Power* **2014**, in press.

[38] W. L. Shaw, R. A. Williams, E. L. Dreizin, D. D. Dlott, Using Laser-Driven Flyer Plates to Study the Shock Initiation of Nanoenergetic Materials, *18th Biennial Intl. Conference of the APS Topical Group on Shock Compression of Condensed Matter*, APS, Seattle, WA, USA, **2013**, in press.

[39] G. C. Egan, K. T. Sullivan, T. LaGrange, B. W. Reed, M. R. Zachariah, in situ Imaging of Ultra-Fast Loss of Nanostructure in Nanoparticle Aggregates, *J. Appl. Phys.* **2014**, *115*, 084903.

[40] J. W. Spears, H. Krompholz, L. L. Hatfield, Sub-Nanosecond Point-Plane Gas Breakdown in a Conical-Shaped Spark Gap, *Digest of Technical Papers-IEEE International Pulsed Power Conference*, **2003**, 1347.

[41] H. Yamashita, K. Yamazawa, Y. S. Wang, The Effect of Tip Curvature on the Prebreakdown Streamer Structure in Cyclohexane, *IEEE Trans. Dielectr. Electr. Insul.* **1998**, *5*, 396.

Received: January 23, 2014
Revised: March 12, 2014
Published online: April 30, 2014

